Available online at www.sciencedirect.com
ScienceDirect
Journal of Nuclear Materials 362 (2007) 181–188
journal of nuclear materials
www.elsevier.com/locate/jnucmat

Helium behaviour and vacancy defect distribution in helium implanted tungsten

A. Debelle *, M.F. Barthe, T. Sauvage, R. Belamhawal, A. Chelgoum, P. Desgardin, H. Labrim

CNRS-CERI, 3A Rue de la Ferollerie, 45071 Orleans cedex 2, France

Abstract

The distribution and the nature of ^{3}He implantation-induced defects in polycrystalline tungsten samples were studied by Positron Annihilation Spectroscopy as a function of implantation fluence. The implanted helium profile was determined by Nuclear Reaction Analysis, and its evolution under different thermal annealings was investigated. Results show that vacancy-like defects are generated along the path of the ions and that their concentration varies directly as the implantation fluence. No helium desorption was observed under any thermal treatments. However, a change in ^{3}He depth profile under specific annealing conditions suggests the formation of nanometric-size He bubbles.

PACS: 66.30.−h; 61.80.Jh; 25.45.−z; 78.70.Bj

1. Introduction

The ultimate goal of fusion research, i.e. in approximately 40–50 years, is to construct and operate an energy generating system based on the simple reaction: $^2\mathrm{H} + {}^3\mathrm{H} \rightarrow {}^4\mathrm{He} + \mathrm{n}$ (14 MeV). The future International Thermonuclear Experimental Reactor (ITER), planned to operate in about 10 years, must prove the scientific and technical feasibility of producing energy by atomic fusion. However, at present, a primordial objective is to define the materials that will be capable of reliable performance under severe burning plasma conditions, which will require the development of grade materials with suitable microstructure and mechanical properties. Indeed, the components inside the fusion reactor will be submitted to a very severe environment, e.g. very high heat flux deposition and particles bombardment, that was not encountered in present-day machines. Tungsten, by its intrinsic physical properties such as low sputtering yield for light elements and good thermo-mechanical behaviour, is a candidate divertor material in controlled fusion experiments.

The divertor will have to face intense neutron, helium and hydrogen isotopes irradiations. The He behaviour in W has already been the focus of many studies in the frame of materials for fusion research [1,2]. Most of the published results deal with the helium behaviour (e.g. desorption, bubble

* Corresponding author. Tel.: +33 2 38 25 57 56; fax: +33 2 38 63 02 71.
E-mail address: debelle@cnrs-orleans.fr (A. Debelle).

0022-3115/$ - see front matter © 2007 Elsevier B.V. All rights reserved.
doi:10.1016/j.jnucmat.2007.01.021

formation) in samples implanted at low energy (in the 1–10 keV range) and higher ion fluences (in the 10^{17} cm^{-2} range). These conditions fit more especially those that encounter the materials that face the He flux at the edge plasma. Besides this important issue, it is also of prime importance to improve the knowledge on the behaviour of homogeneously introduced He and H in W, as it could be if this latter is used in the post ITER generation of fusion reactor, i.e. in the DEMO system. Indeed, in this reactor, the high flux of 14 MeV neutrons will cause the continuous production of H and He by (n, p) and (n, α) nuclear reactions. In this case, it is especially crucial to study the He and H interaction with irradiation-induced defects. An experimental study, of which aim is to better understand the He migration processes, and more precisely the role of the vacancy defects and of the grain boundaries in implanted polycrystalline W, has just began at the CERI-Orléans. The present paper relates the preliminary results concerning the characterisation of the defects created by ^{3}He implantations in polycrystalline W samples and the helium behaviour after different thermal treatments. Most of the time, the two aspects are treated separately. In the present work, Positron Annihilation Spectroscopy (PAS), for the detection and identification of point defects on an atomic scale, and Nuclear Reaction Analysis (NRA), for the determination of helium profiles, are both used to handle these two topics.

2. Experimental details

2.1. Samples preparation

Polycrystalline 99.95% pure W samples 150 μm thick cut out of commercial laminated foils were used for this study. Density of the samples is 18.97 ± 0.02 g cm^{-3}, that is, compared to the theoretical one, about 2% lower. In order to eliminate manufacturing-induced surface defects, all the samples were mechanically polished until diamond paste with 0.2 μm grains. The average surface roughness after the polishing, as measured with a mechanical profilometrer, was strongly improved; a value of 0.2 ± 0.1 μm was found in polished samples instead of ~2 μm before the preparation. Samples that were analysed by PAS were also submitted to a thermal treatment, 1773 K during 1 h under Ar–H_2 atmosphere in a tubular furnace, to reduce the large concentration of laminating/polishing-induced defects in the region probed by the positrons. This annealing allowed to eliminate a large part of defects, as will be explained latter. Grain size is typically a few microns for polished samples, and for the annealed ones, a recrystallisation occurred, leading to an increase of the grain size up to ~20–25 μm.

2.2. ^{3}He implantations

^{3}He implantations have been performed with the 3.5 MV Van de Graaff accelerator at the CERI-Orléans (France). Implantations were carried out by focusing the 8×8 mm^2 primary ion beam to a 1×1 mm^2 one and by sweeping it over the surface sample to ensure a homogeneous fluence. Three He fluences have been applied, 10^{15}, 10^{16}, and 5×10^{16} cm^{-2}, with a mean flux ranging from 10^{11} to 10^{12} cm^{-2} s^{-1}. Samples probed by positrons were implanted at 800 keV, in order to obtain a projected range beyond the positrons implantation profile (see Fig. 1(a) and below), and samples analysed by NRA

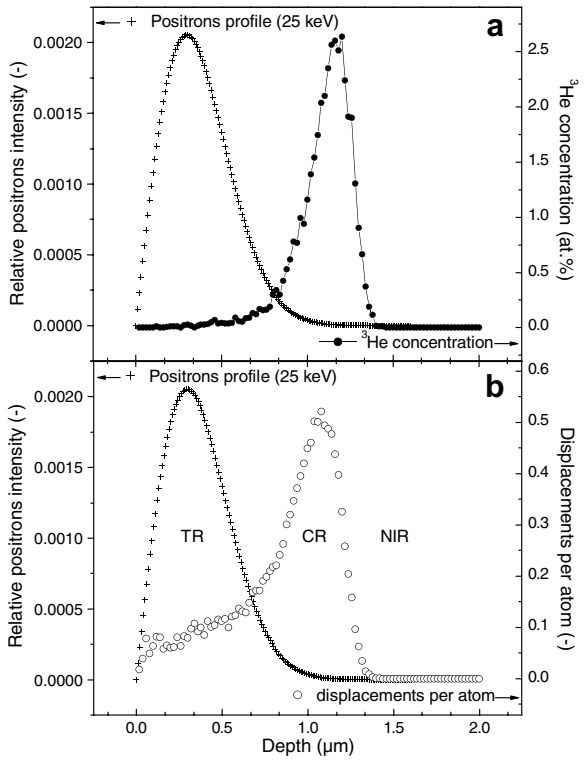

Fig. 1. SRIM calculations of (a) the implantation profile of 800 keV ^{3}He ions implanted at a 5×10^{16} cm^{-2} fluence at RT in tungsten; (b) corresponding displacements profile, taking a displacement threshold energy of 90 eV. TR, CR and NIR respectively represent the tracks, cascades and non-implanted regions (see text). The implantation profile of 25 keV positrons in tungsten is also represented in both (a) and (b).

were implanted at 500 keV for a better resolution in the He depth profiling. During all experiments, the mean temperature of the sample holder was below ~333 K.

The theoretical helium implantation profiles, as determined from SRIM calculations [3], are presented in Figs. 1(a) and 3(a), for the 800 keV and 500 keV energies respectively. For a ^{3}He implantation fluence of 10^{16} cm^{-2} the maximum 500 keV ^{3}He concentration, situated at 0.78 μm, is 0.6 at.% (see Fig. 3(a)). For an implantation at 800 keV at a ^{3}He fluence of 5×10^{16} cm^{-2}, the largest one, the number of displacements per W atom (dpa), as calculated with the SRIM code taking a displacement threshold energy in W of 90 eV [4,5], is plotted in Fig. 1(b). The dpa damage is defined as the total displacements over the W atomic density. In the Fig. 1(b), CR is the cascades region, corresponding to the region where incident ions mainly interact with atoms of the solid via nuclear collisions and finally stop into the lattice; TR denotes the tracks region, localized between the surface and the nuclear cascades region, and corresponding to the zone where ions slow down mainly by electronic energy loss processes; NIR is the non-implanted region. The theoretical maximum dpa damage, located at ~1.08 μm depth, is ~0.55 for the 5×10^{16} cm^{-2} helium implantation fluence. Note that SRIM code does not take into account any recombination process, so this value must be considered as an upper value.

2.3. Positron annihilation spectroscopy: Doppler broadening spectroscopy measurements

The positron annihilation spectroscopy study was carried out using an accelerator of positrons, built in Orléans at the CERI, that delivers a monoenergetic positron beam of variable kinetic energy (for a complete description see [6]). A Doppler Broadening Spectrometer (DBS) is coupled to the positron accelerator and allows to probe vacancy defects in numerous types of materials. The measurement system is a standard gamma-spectroscopy system equipped with a high purity germanium detector that offers a high energy resolution (<1.3 at 511 keV) and a high efficiency (>25% at 1.33 MeV). The positron–electron pair momentum distribution has been measured at room temperature (RT) by recording the Doppler broadening of the 511 keV annihilation line characterised by the S and W integral parameters. S is defined by the ratio of the area calculated around the maximum of the peak in the momentum window ($0 - |2.80| \times 10^{-3} m_0 c$), over the total number of annihilations. The m_0 and c parameters are respectively the rest mass of the electron and the speed of light. This S fraction corresponds to annihilations with low momentum electrons, thus more predominantly with valence electrons. W is defined by the ratio of the area calculated at the wings of the peak in the momentum windows ($|10.61| - |26.35| \times 10^{-3} m_0 c$), over the total number of annihilations. This W fraction corresponds to annihilations with high momentum electrons, thus it is essentially related to positron annihilations with core electrons. By varying the incident positrons energy, the depth dependence of S and W can be obtained. In the present case, $S(E)$ and $W(E)$ were recorded in the range 0.5–25 keV, the energy being changed in 0.5 keV steps; the total count rate was chosen so that a good statistic is ensured. This energy range corresponds to a mean positrons implantation depth in W comprised between approximately 0.4 and 300 nm. Note that the full-width-at-half-maximum of the implanted positrons distribution increases with the energy, to reach ~380 nm at 25 keV. At this energy, positrons probe up to ~700 nm under the tungsten surface. Thus, as can be seen in Fig. 1(a), positrons do not probe the ^{3}He ions stopping zone. A UO_2 disk, labelled B23, polished and thermally annealed at 1973 K during 24 h in humid Ar–H_2 atmosphere, was chosen as a sample reference. Indeed, in this disk, S and W values remain constant, and close to the tungsten ones, over a large energy range, 5–25 keV ($S_{B23} = 0.3713$ and $W_{B23} = 0.0791$). This reference sample allows to check the reproducibility of the measurements, especially the stability of the positron beam and of the DBS system. For the reader convenience, the positron annihilation characteristics S and W, obtained with the same system in a more used material, e.g. the silicon, are given in [7]. Note that each material exhibits specific S and W values, signature of the momentum electrons distribution in the lattice in the absence of vacancy defects. Thus, it is important to keep in mind that S increases and W decreases when positrons are trapped and annihilate in vacancy defects.

Hereafter, a modified version of VEPFIT [8], which combines the calculation of the positrons implantation and their diffusion, is used to consistently fit the $S(E)$ and $W(E)$ curves. Note that the data below 2.5 keV are discarded because in this energy range, the positrons migration is not due, in the present case, to a diffusion process.

2.4. He depth profile and lateral distribution

The He lateral distribution and the He depth profile were determined by using the DIADDHEM (set-up for He and ^{2}H diffusion analysis in materials) device. This recent apparatus is installed at the end of one of the beam lines of the Van de Graaff accelerator at the CERI. This system includes the features required for the routine application of Ion Beam Analysis techniques applied to materials analysis. Its originality resides in the coupling of the ^{3}He(d, α)^{1}H NRA technique with an electronic bombardment furnace allowing *in situ* regulated heating in a wide range of temperature $300 < T < 1600$ K. Thus, this set-up offers the advantage to perform He cartographies, depth profiling and *in situ* helium desorption measurements at various stages of an annealing process.

In the present study, probed deuterons energy was fixed at 700 keV. Homogeneity of the lateral implanted helium distribution was investigated by performing cartographies of the samples. In this analysis mode, only protons transmitted through the W samples are detected at a 0° angle from the incident deuteron beam. The lateral resolution was in the present case restricted to 0.5×0.5 mm^2 due to the probe beam spot size. For helium depth profiling, the two reaction products, ^{1}H and α, are detected in coincidence. Details of the method are reported elsewhere [9,10]. The He depth profile is finally determined from the fitting of the α experimental spectrum using the SIMNRA program [11] in which the Ziegler–Biersack–Littmark (ZBL) stopping powers and the ^{3}He(d, α)^{1}H cross-section measured by Sauvage et al. [10] are integrated. This program allows the fitting of the experimental data assuming a sequence of tungsten layers with an evolutive helium concentration. The results obtained by the coincidence technique show that the profile at a depth over 1 μm can be resolved at a scale of 0.1 μm with a ^{3}He detection limit close to 0.01 at.%. Such resolution is impossible to achieve in a standard detection mode, where the alpha particles and the protons are separately detected.

3. Results and discussion

3.1. Implantation-induced defects studied by DBS

The evolution of the normalised low, S, and high, W, momentum annihilation fractions as a function of the positrons energy for a mechanically polished polycrystalline W sample is presented in the Fig. 2(a) and (b), respectively. The values of $S(E)$ and $W(E)$ remain constant, respectively at 0.416(6) and 0.058(6). It traduces a very weak positron diffusion length, probably linked to a strong trapping of positrons at defects, in particular at vacancy-type defects. The polished samples were thermally annealed at 1773 K for 1 h under an Ar–H_2 atmosphere, which allowed to strongly reduce the defects concentration, since the $S(E)$ (resp. $W(E)$) values for the highest positrons energy, so the values characterising the bulk of the material, are largely lower (resp. higher) than the ones obtained before the thermal treatment. A fitting of experimental data, represented in Fig. 2(a) and (b), with the diffusion model proposed by the VEPFIT program, taking into account a unique homogeneous layer, gives the following volume annihilation characteristics: $S = 0.368(3)$ and $W = 0.090(6)$; the effective positron diffusion length is found to be ~32 nm, which

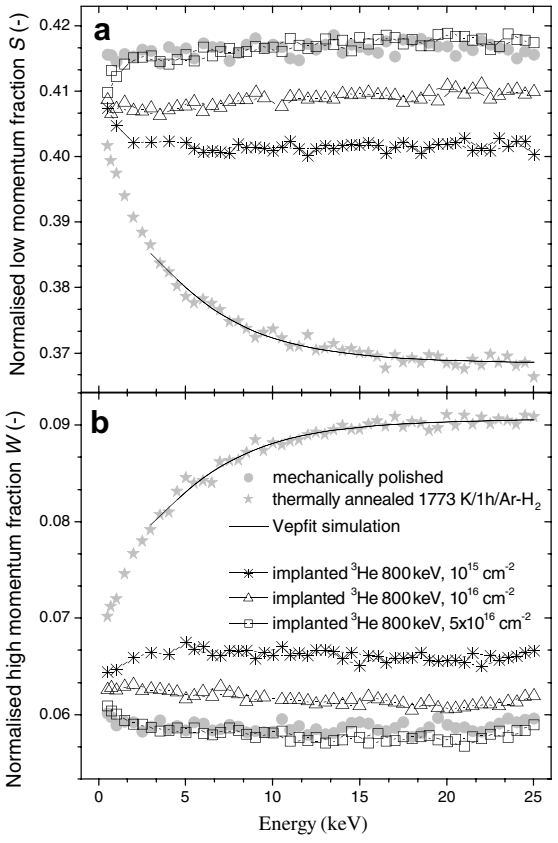

Fig. 2. Evolution of the positrons annihilation characteristics in different tungsten samples (see legend) as a function of the positrons energy: (a) normalised low momentum fraction S, and (b) normalised high momentum fraction W.

appears relatively small compared to the values available for W in the literature [12,13], that is to say 80–140 nm. Therefore, despite the visible improvement of the samples quality after the thermal treatment, better annealing conditions could be found. Nonetheless, it is now possible to investigate the evolution of the annihilation characteristics of the tungsten samples after helium implantation. $S(E)$ and $W(E)$ for three implantation fluences at 800 keV are plotted in Fig. 2(a) and (b). The S and W values drastically increase and decrease respectively, which clearly indicates that positrons detect, whatever the fluence, the presence of vacancy-type defects generated during implantation. The slow positron beam probe W samples up to ~700 nm under the surface, which corresponds to the track region. Consequently, defects are created all along the path of the implanted helium ions. This appears in concordance with the SRIM results that effectively indicate that the W atoms displacements can lead to the formation of vacancies in this region (see Fig. 1(b)).

With the present implantation conditions, radiation damage is expected to be small: SRIM calculations indicate, for a ^{3}He fluence of 5×10^{16} cm^{-2}, an average dpa damage of 0.1 in the region probed by the positrons. Moreover, from the weighted average recoil spectrum, it is possible to determine an energy characterising the radiation damage [14]. In the present case, this energy, estimated for the whole radiation damage zone, that means the track and the cascade regions, is ~500 eV, which means that, based on SRIM calculations, a W recoil displaces in average only 3 atoms. This value must be lowered in the track region. Furthermore, vacancies are not mobile in tungsten at RT [15]. Finally, it is likely that principally mono-vacancies are created. Positron lifetime measurements, associated with the determination, by DBS measurements, of the S and W annihilation characteristics of positrons in irradiated tungsten as well as in the tungsten lattice free of vacancy defects, should confirm this result. This work is actually in progress, but it requires, as already mentioned, to find annealing conditions that allow to obtain W samples without intrinsic defects, or at least with a concentration lower than the PAS technique detection limit. Another important result is that S (resp. W) increases (resp. decreases) with the implantation fluence, which implies a higher defects concentration or/and a change in the defects nature. For the same reasons than those previously evoked, an increase in the defects concentration is rather expected.

3.2. ^{3}He behaviour under thermal treatments investigated by NRA

As previously mentioned, implantations were achieved on laminated/polished samples which were not submitted to any thermal treatment. Therefore, they contain a large concentration of vacancies as shown by PAS measurements (see above). In order to get better insight of the helium migration processes in implanted tungsten, with the aim, forward, to determine a reliable 'effective' diffusion coefficient, thermal annealings were performed; two different conditions were chosen: *in situ*, at 1473 K during 70 min under vacuum directly in the NRA analyses chamber, and *ex situ*, at 1773 K during 60 min under a Ar–H_2 atmosphere in a tubular furnace.

The lateral helium distribution before and after both types of annealing in several representative samples was determined by recording the protons signal over a 3×3 mm^2 area. The cartographies (not shown here) indicate an homogeneous lateral helium distribution, before as well as after the two different annealings; in the same time, no blisters nor exfoliation were observed by optical and scanning electron microscopies. The protons average signal before and after annealing was nearly identical, which traduces that no helium desorption occurred during any annealing conditions. Recording of the protons signal was also performed during the whole *in situ* annealings. The protons signal remained constant, in other words no helium desorption was noticed, at none of the two studied fluences, 10^{15} and 10^{16} cm^{-2}.

^{3}He depth profile was only determined on the 10^{16} cm^{-2} implanted samples. Obtaining a profile with the same statistics on the 10^{15} cm^{-2} implanted ones would have been time-consuming. Note that the reproducibility of the alphas spectra and a 100% coincidence rate were verified on several samples. Fig. 3(a) shows the ^{3}He profile of a 10^{16} cm^{-2} implanted sample. Helium is detected up to a ~1.2 μm depth while the maximum helium concentration, 0.41 ± 0.01 at.%, is located at 0.78 ± 0.05 μm. If the maximum of this experimental distribution is at the same position than the theoretical one deduced from SRIM calculations, its width appears larger and the maximum concentration lower, a difference usually found and attributed to an incorrect evaluation of the straggling phenomena by the SRIM program. The total amount of retained helium deduced from this measurement

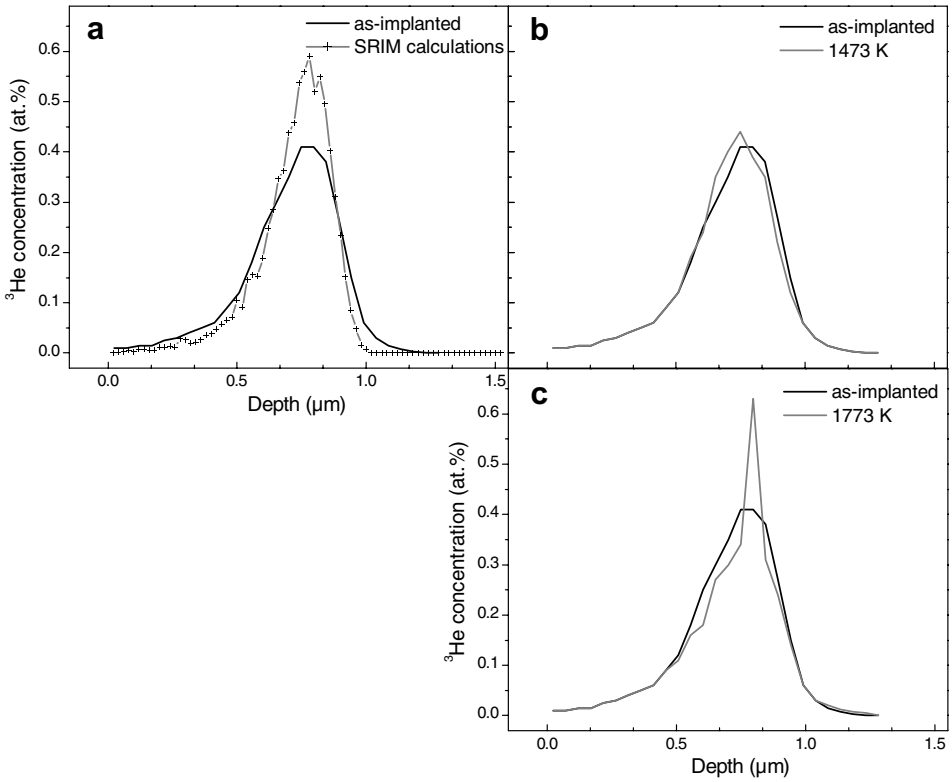

Fig. 3. (a) Theoretical (SRIM calculations) and experimental distributions of 500 keV ^{3}He ions implanted at a 10^{16} cm^{-2} fluence in tungsten at RT; (b) evolution of the experimental implantation profile after a thermal annealing at 1473 K during 70 min under vacuum and (c) after a thermal annealing at 1773 K during 1 h under Ar–H_2 atmosphere.

reaches a ^{3}He fluence of $(9.85 \pm 0.3) \times 10^{15}$ cm^{-2}. This result traduces the accuracy of the cross-section determination and of the charge measurements during the helium implantation and the depth profile. But this result also suggests a possible helium trapping. Indeed, before reaching a thermal equilibrium with the lattice, the implanted helium ions could have migrated interstitially to the surface, since its migration energy in W at RT is very low, ~0.24 eV [16]. Thus, since no helium was released during implantation, helium ions could have been trapped at, e.g., vacancy defects induced by the preparation method and by irradiation. The strong attractive interaction of helium in metals with vacancies is indeed a well established phenomenon.

The helium profiles after the thermal treatments are presented in the Fig. 3(b) and (c). A slight difference between the spectra before and after the annealing at 1473 K under vacuum can be noticed. Despite the perfect reproducibility of the alphas spectra and the 100% coincidence rate, it appears more reasonable to consider it as negligible. Thus, this means that no He desorption nor even diffusion is observed with these annealing conditions. On the contrary, a drastic change in the helium profile after the annealing at higher temperature, 1773 K under Ar–H_2 atmosphere, is clearly observed. Some of the He atoms around the as-implanted maximum concentration migrate, which is translated into the apparition of a sharp peak at the depth of the maximum observed in the as-implanted profile. The induced He over-concentration, estimated at ~0.62 at.%, strongly suggests the formation of helium bubbles. Such a phenomenon has already often been observed [17–20]. A single 50 nm W layer, which corresponds to He depth resolution of the technique at 0.8 μm, allows to accurately reproduce this over-concentration. Therefore, this thickness value defines the upper bubbles size. The ^{3}He surface density contained in this sharp peak is estimated to 8×10^{14} cm^{-2}, which represents 8% of the implanted fluence. The estimation of the volume concentration of helium in bubbles cannot be provided because the average size of the bubbles is

unknown. Nevertheless, it is planned to achieve a Transmission Electron Microscopy study to investigate the assumed formation of nano-scaled bubbles in the samples implanted at 10^{16} cm^{-2}, but also in those implanted at a lower fluence, that is in the present case 10^{15} cm^{-2}.

Finally, no helium desorption, with a relative precision of ~3%, was observed in any annealing conditions. However, as already mentioned, He is mobile at RT, even in the presence of trapping sites. Indeed, a 10^{-10} m^2 s^{-1} effective helium diffusion coefficient in tungsten containing a large concentration of vacancy trapping sites, in the temperature range ~850–1700 K, was estimated by Takamura [21]. In the present case, that is to say annealings during ~1 h at 1473 or 1773 K, a helium migration over ~6 μm could have occurred. The fact that no migration was observed well supports the assumption of the precipitation of helium bubbles. Gilliam et al. [17] did neither observe, in similar implantation conditions (1.3 MeV, 5×10^{16} cm^{-2}), any change in helium retention after flash annealings at 2273 K. They also attributed their results to the formation of helium bubbles. From these results, the following scheme can be drawn: during implantation, highly stable helium–vacancy complexes are created. Then, during annealing, it seems most likely that these complexes migrate and coalesce to form bubbles, since these latter are only observed when increasing the implantation fluence. Grain boundaries act as nucleation sites for bubbles when a critical concentration is reached, in particular at high implantation fluences [17,20]. Thus, bubble growth could have been favoured by bubble migration along grain boundaries. Furthermore, during the thermal treatments, a grain growth might have occurred. A dragging effect of helium by the moving grain boundaries could also have contributed to the bubble growth [22].

4. Summary

The distribution and the nature of ^{3}He implantation-induced defects in polycrystalline tungsten samples was studied by Doppler Broadening Spectroscopy measurements combined with the use of a slow positron beam. This allowed the investigation of the track region of the ^{3}He ions where, although the implantation conditions induced low radiation damage, vacancy-type defects, which are most likely mono-vacancies, are detected. Moreover, an increase in the defects concentration as a function of the fluence is noticed. The implanted helium behaviour under thermal annealing was studied by NRA. In any annealing conditions, no helium desorption is detected for both 10^{15} and 10^{16} cm^{-2} ^{3}He implantation fluences. However, the presence of helium bubbles is observed in W samples implanted at the highest fluence, 10^{16} cm^{-2}. These results strongly suggest that He atoms are trapped at vacancies during implantation, thus forming stable vacancy–helium complexes, which tend to form bubbles during thermal treatments when increasing the implantation fluence.

Acknowledgment

This study is financially supported by the department for the controlled fusion (DRFC) of CEA in the framework of the Sixth European *EURATOM* Framework Programme.

References

[1] Proceedings of Plasma–Surface Interactions in Controlled Fusion Devices 15, J. Nucl. Mater. 313–316 (2003) 92, 97.
[2] Laser Fusion Materials, Special issue on Materials Development for Inertial Fusion Energy, J. Nucl. Mater. 347 (2005) 289.
[3] J.F. Ziegler, J.P. Biersack, U. Littmark, The Stopping and Range of Ions in Solids, Pergamon, New York, 1985 <www.srim.org>.
[4] Standard Practice for Neutron Radiation Damage Simulation by Charge-Particle Irradiation, E521-96, Annual Book of ASTM Standards, vol. 12.02, American Society for Testing and Materials, Philadelphia, 1996.
[5] P. Lucasson, in: Proceedings of the Conference on Fundamental Aspects of Radiation Damage in Metals, CONF 75-1006-P1, Gatlinburg, 1975, p. 42.
[6] P. Desgardin, L. Liszkay, Marie-France Barthe, L. Henry, J. Briaud, M. Saillard, L. Lepolotec, C. Corbel, G. Blondiaux, A. Colder, P. Marie, M. Levalois, Mater. Sci. Forum 363–365 (2001) 523.
[7] P. Desgardin, M.-F. Barthe, E. Ntsoenzok, C.-L. Liu, Appl. Surf. Sci. 252 (2006) 3231.
[8] A. van Veen, H. Schut, J. de Vries, R.A. Hakvoort, M.R. Ijpma, in: P.J. Schultz, G.R. Massoumi, P.J. Simpson (Eds.), Positron Beams for Solids and Surfaces, AIP, New York, 1990, p. 171.
[9] S. Guilbert, T. Sauvage, P. Garcia, G. Carlot, M.-F. Barthe, P. Desgardin, G. Blondiaux, C. Corbel, J.P. Piron, J.M. Gras, J. Nucl. Mater. 327 (2004) 88.
[10] T. Sauvage, H. Erramli, S. Guilbert, L. Vincent, M.-F. Barthe, P. Desgardin, G. Blondiaux, C. Corbel, J.P. Piron, F. Labohm, J. Van Veen, J. Nucl. Mater. 327 (2004) 159.
[11] M. Mayer, SIMNRA User's Guide, Report IPP 9/113, Max-Planck-Institut fur Plasmaphysik, Garching, Germany, 1997, <http://www.rzg.mpg.de/~mam/>.
[12] R. Paulin, R. Ripon, Appl. Phys. 4 (1974) 343.
[13] I.K. Mac Kenzie, in: Positron Solid-state Physics: Proceedings of the International School of Physics 'Enrico Fermi',

W. Brandt, A. Dupasquier (Eds.), Varenna, Italy, 1983, p. 196.
[14] R.S. Averback, J. Nucl. Mater. 216 (1994) 49.
[15] I.A. Schwirtlich, H. Schultz, Phil. Mag. A 42 (1980) 601.
[16] W.D. Wilson, C.L. Bisson, M.I. Baskes, Phys. Rev. B 24 (1981) 5616.
[17] S.B. Gilliam, S.M. Gidcumb, N.R. Parikh, D.G. Forsythe, B.K. Patnaik, J.D. Hunn, L.L. Snead, G.P. Lamaze, J. Nucl. Mater. 347 (2005) 289.
[18] V.S. Subrahmanyam, P.M.G. Nambissan, P. Sen, Solid State Commun. 89 (1994) 523.
[19] M. Tokitani, M. Miyamoto, D. Koga, K. Tokunaga, T. Fujiwara, N. Yoshida, S. Masuzaki, N. Ashikawa, T. Morisaki, M. Shoji, A. Komori, J. Nucl. Mater. 337–339 (2005) 937.
[20] N. Hashimoto, J.D. Hunn, N.R. Parikh, S.B. Gilliam, S.M. Gidcumb, B.K. Patnaik, L.L. Snead, J. Nucl. Mater. 347 (2005) 307.
[21] Takamura, Rad. Effects Lett. 43 (2) (1979) 69.
[22] A.M. Brass, A. Chanfreau, J. Chêne, Metal. Mater. Trans. 25A (1994) 2117.